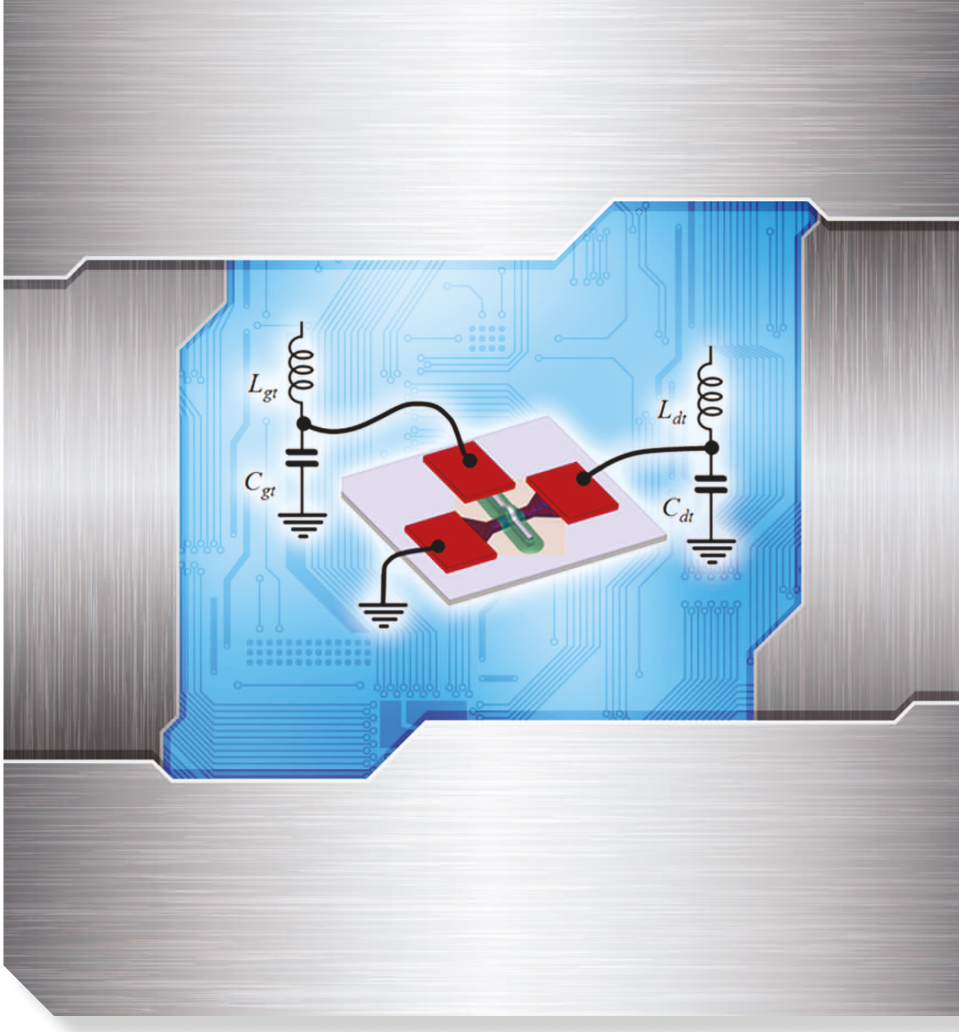

CIRCUIT IMAGE LICENSED BY INGRAM PUBLISHING

Dual-Port Reflectometry Technique

Charge identification in nanoscaled single-electron transistors.

ALEXEI O. ORLOV, PATRICK FAY, GREGORY L. SNIDER, XAVIER JEHL, SYLVAIN BARRAUD, AND MARC SANQUER

Digital Object Identifier 10.1109/MNANO.2015.2409411
Date of publication: 7 April 2015

RADIO-FREQUENCY REFLECTOMetry (RFR) is a technique that was developed to characterize the properties of transmission lines by observing reflected waveforms. Today, it is widely used in a variety of applications, ranging from the detection of faulty wires in cables [1] and objects buried in the ground [2] to soil moisture detectors [3] and the measurement of dielectric properties of blood [4]. Recently, one important application of this technique, which requires a very small amount of applied power, was developed for the characterization of electronic nanostructures [5]. In this implementation, a microwave radio-frequency (RF) signal is sent to a resonator coupled to the specimen to be studied. If in a specimen the change of some external parameter (e.g., gate voltage) leads to a change of an active [Figure 1(a)] or a reactive (typically, capacitive) load [Figure 1(b)] to the resonator, the self-resonance is affected, resulting in a change of magnitude [Figure 2(a)] and phase [Figure 2(b)] of the reflected signal. If an impedance matching condition is achieved, the modification of the specimen parameter (e.g., the increase of its resistance) will lead to a very significant change in the reflection coefficient Γ [Figure 2(a)]. Here, we discuss two important applications of the RFR technique on nanoscale devices.

First, RFR provides a method for fast (<100 ns) and broadband (in excess of 100 MHz) sensing of single-electron transistors (SETs) [5] and quantum point contacts (QPCs) [6], which are essential readout elements for promising new technologies such as spin quantum bits [7]–[9]. By contrast, the traditional methods of probing these types of devices by measuring changes in their conductance or resistance suffer from very limited bandwidth (<1 MHz) due to the high impedance of the devices and parasitic input capacitance of the sensing amplifier. In an

Radio-frequency reflectometry is a technique that was developed to characterize the properties of transmission lines by observing reflected waveforms.

RFR SET setup [5], the input RF sine wave (with a frequency in the range of 10^8–10^9 Hz) is reflected from a tank circuit, typically consisting of a lumped inductor and a parasitic capacitor to ground, acting as an impedance transformer, and the device under test (an SET or QPC) acting as the load. The main purpose of the inductor-capacitor (L-C) impedance transformer is to transform the high impedance of the device under test closer to a standard transmission line resistance, e.g., 50 Ω. Because the impedance transformer typically used in an RFR setup is a resonant circuit, it also provides frequency selectivity, attenuates unwanted signals away from the resonant frequency, and suppresses "pink" $1/f$ noise [10].

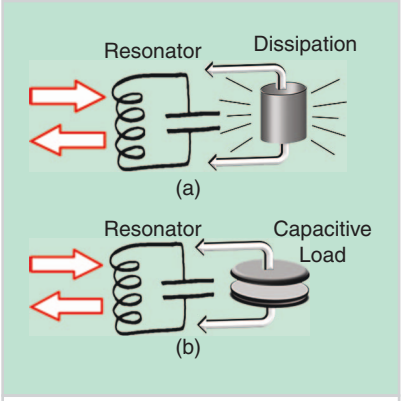

FIGURE 1 RF reflectometry sensing. Here, a change in the specimen characteristics, such as (a) the active resistance or (b) the reactive load (capacitance shown), leads to changes in resonator characteristics and, thus, changes in the phase and amplitude of reflected signal.

The second class of applications is the use of RFR-based spectroscopy to enable researchers to "look inside" devices to understand the intricate physical mechanisms of transport on the nanoscale. RFR in this case is used as a unique characterization tool for studying the properties of these devices and the materials of which they are composed. For this class of RFR application, speed and wide bandwidth are typically of lesser concern than obtaining the highest possible sensitivity. Even small changes in the device capacitance, for example, as might arise from a single defect level, may be sufficient to produce a detectable signal. The role of the resonator is to increase the sensitivity of the reflected signal (i.e., the magnitude and phase) to changes in the device impedance, thereby easing the detection of small changes (e.g., caused by single-electron charging of an SET island or trapping/detrapping effects near it).

The tools developed in the process of pursuing these two applications are complementary so that development in one leads to the progress in the other. For example, improvements in the charge sensitivity of the RF SET qubit readout enhance the detection capabilities of the charged defect detecting technique.

TRANSPORT SPECTROSCOPY IN MESOSCOPIC SYSTEMS

Transport spectroscopy is a characterization technique where electron transport through the sample is measured as a function of one or more parameters. The information about electron transport is typically revealed by analyzing low-frequency differential conductance "maps"—dependences of differential conductance $G = dI_{ds}/dV_{ds}$ on two variables such as gate and source–drain voltages $G(V_g, V_{ds})$. This technique is widely used for the characterization of mesoscopic structures (e.g., quantum dots, SETs, and QPCs) [11]. The characteristic features in such maps, the so-called Coulomb diamond plot in the SETs, enable the determination of the type of transport mechanism (e.g., resonant tunneling and quantum or classical charge transfer) and device parameters such as gain, charging energy, and gate sensitivity. At the same time, the deviations from ideal models are used to identify various charged defects (e.g., single donors and dislocations [12]). Clearly, a measurable dc current between the source and the drain of the device is required to obtain these maps.

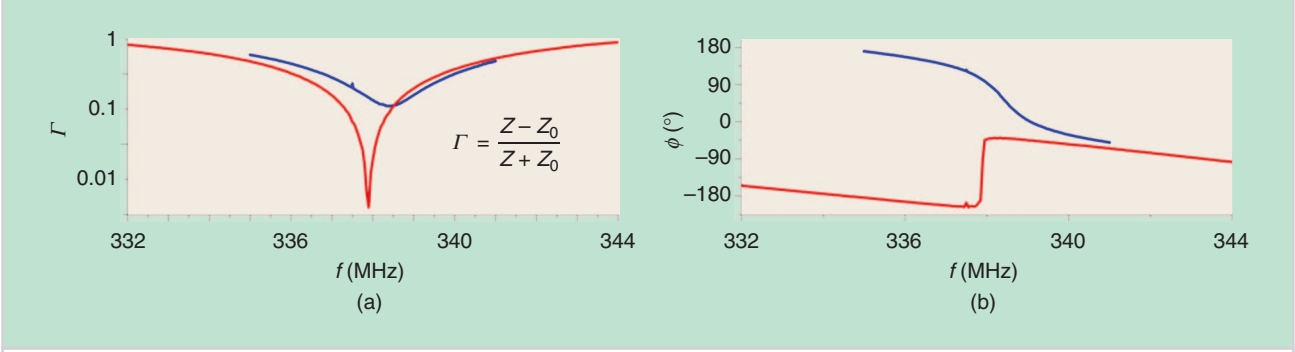

FIGURE 2 The change in the (a) magnitude and (b) phase of the signal reflected from the tank circuit caused by a change in the channel resistance of the HJFET coupled to it. The fully depleted FET channel, $R \approx 500\,k\Omega$ (blue curves, $V_g = -0.85\,V$); matching condition achieved, $R_{eff} = L/CR_{ch} \approx Z_0 = 50\,\Omega$; here, $R_{ch} \approx 120\,k\Omega$ (red curves, $V_g = -0.81\,V$).

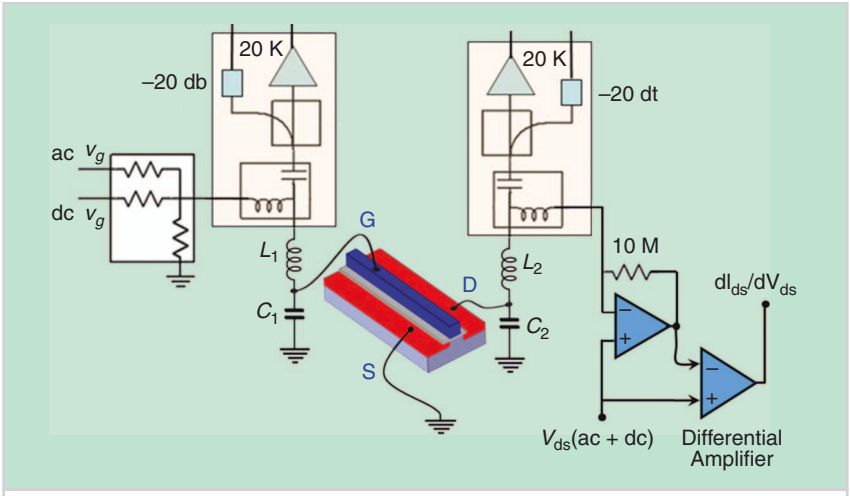

FIGURE 3 A simplified circuit diagram of the dual-port RFR setup. Two tank circuits are connected to the gate and drain of the device. The dc biases and modulation signals are applied through inductor inputs of the bias tees. RF signals are supplied through the directional couplers, and reflected signals are picked up by the preamplifiers. The sample is bonded to a printed circuit board with two surface mount inductors. In conjunction with the parasitic pad capacitances to ground, it forms two separate resonant tank circuits, one at the drain and one at the gate. The sample is cooled to ≈ 3.5 K, and the preamplifiers are cooled to ≈ 20 K using a closed-cycle refrigerator.

Here, RFR-based spectroscopy offers a versatile spectroscopic tool that is particularly useful for the identification of single-electron charging in nanoscale devices. Unlike dc spectroscopy, it does not require any dc current flow and, thus, not only provides a means for detection based on the change of conductance but also enables the detection of electron processes occurring in systems with no dc current flow, for example, electron charging of a capacitor through a single tunnel junction [13], [14].

gate modulation and hysteretic effects was reported in [15], and the detection of a charged defect leading to a transport blockade in an SET was observed in [16]. In both cases, the origins of the charge reflection mechanisms were determined by analyzing the maps of reflected signals and comparing them to simulations.

Since in the RFR configurations reported to date the reflected signal was acquired from only one port (e.g., a drain [5], [10], [16] or a gate [17]–[19]), pinpointing the spatial location of a particular charging process is an elaborate and indirect process.

The technique we describe here not only detects electron charging in nanostructures but also enables the spatial identification of the location of the charging events. The idea is to use two independent channels to perform RFR measurements on a three-terminal device. Single-electron charging events occurring in the device near the threshold, where it can be treated as a passive network with no internal gain, result in very small variations of the reflection coefficient. Therefore, the farther the location of the charging event from a specific port, the stronger the attenuation of the associated reflected signal. By monitoring the reflection from two ports and comparing the reflected signals, one can positively identify the location of the specific events. In the following section, we will illustrate the applications of this technique for an off-the-shelf short-channel FET and for an ultrasmall nanoscale silicon (Si) single-hole transistor (SHT).

> The role of the resonator is to increase the sensitivity of the reflected signal to changes in the device impedance, thereby easing the detection of small changes.

REFLECTOMETRY FOR DEFECT IDENTIFICATION

In recent publications, we reported two charging processes occurring in nanoscale metal-oxide-semiconductor field-effect transistors (FETs) identified by means of RFR spectroscopy. Charge trapping in the polysilicon gate leading to unwanted

EXPERIMENTAL RESULTS AND DISCUSSION

MEASUREMENT SETUP

To implement the proposed technique, we built a dual-channel reflectometer, the schematics of which are shown in Figure 3. Each channel contains a bias T, a directional coupler with an attenuator, and a cold preamplifier that are connected to the two tank circuits. The resonant frequencies of the two tank circuits are in the range of 0.3–1 GHz. To increase the signal-to-noise ratio, an amplitude modulation technique is used, where a small signal at a frequency $f_M \sim 2$ kHz is applied to the gate. Homodyne detection with a quadrature demodulator is used to recover the modulated signals. After demodulation, the sidebands at f_M are rectified with two lock-in amplifiers to recover full vectors of the signals proportional to the derivatives of the reflection coefficients $d\Gamma_{drain}/dV_g$ and $d\Gamma_{gate}/dV_g$, respectively. In addition to this, the low-frequency differential conductance was measured simultaneously with the reflected signals using standard lock-in amplifier techniques.

TESTING THE METHOD WITH GALLIUM ARSENIDE FET

Electron transport in a heterojunction FET (HJFET) with a short ($\leq 0.3\,\mu$m) and wide ($> 100\,\mu$m) gate offers an opportunity to study a number of interesting physical processes near the conductance threshold. At a high electron density, these devices act as high-speed amplifiers, taking

advantage of the high mobility of electrons traveling through the channel. The high electron density provides screening of the random fluctuation potential from the ionized impurities [20]. This situation changes dramatically near the threshold, when the screening of electrostatic potential fluctuations breaks down. A number of mesoscopic effects, including Coulomb blockade, resonant tunneling, and quantum ballistic transport, can be observed in the transitional region from a fully depleted to a fully conducting channel. In gate-controlled conducting channels with large width-to-length (W/L) ratios, a percolation path is first formed in a region with the lowest electrostatic potential and the highest electron density [21], [22] due to large-scale potential fluctuations caused by random dopant distribution. As electron density under the gate increases, there is a high probability that a random "dot" (or several dots) connecting the source and drain shown in Figure 4 may form in this region. At a low temperature ($T < 10$ K for the devices discussed here), transport through this dot is governed by a Coulomb blockade [23] or resonant tunneling through one or several localized states [24]. Then, as the electron population increases, the depleted regions acting as tunnel barriers disappear due to the increased electron population, and the dot merges with the source and drain regions, forming a narrow constriction. In short-channel devices, when $L < l$ (where l is the electron mean free path), electrons can travel through such constrictions quasi-ballistically, leading to one-dimensional conductance quantization [25]. In addition, a number of isolated puddles, which are tunnel-coupled to the source and drain but not contributing to the dc current, become populated until a continuous percolation path forms between the source and the drain. (A crude analogy would be water filling a potential landscape—water first accumulates in isolated puddles before merging into a stream.) This process of puddle formation—population with electrons of isolated dips in a potential profile—cannot be traced by means of conventional transport spectroscopy as there is no dc current associated with it. By contrast, these charging events can be detected with the RFR technique because, at a low temperature, the charge population of an isolated puddle coupled to a source or drain is also governed by a Coulomb blockade and is similar to the charging of a single electron box—a structure composed of a single tunnel junction and one (or more) nonleaky capacitors [26]. The energy price of electron travel associated with this process leads to power dissipation that is detectable by RFR, which was recently demonstrated in [14].

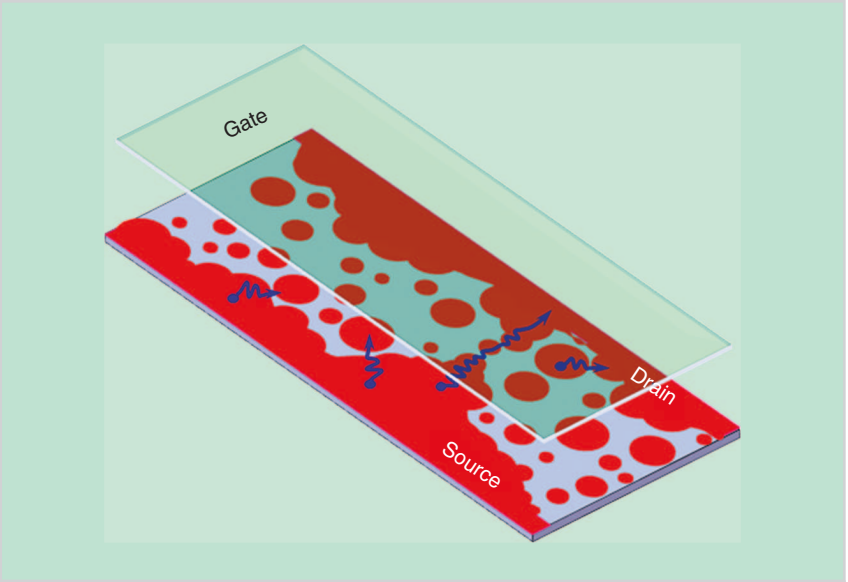

FIGURE 4 An image showing the various charging processes guided by the Coulomb blockade for a wide-channel HJFET at a low temperature. Several charging processes are shown, including electron hopping to isolated localized states near the source and drain and electron transport from source to drain through a "dot" created by the random fluctuation potential. The red color corresponds to areas of high electron density under the gate, and the depleted regions are colored gray.

Here, we performed the dual-port RFR spectroscopy using a device with gate length $L < 0.2\,\mu$m and gate width $W = 160\,\mu$m (NE3210S01). The experimental results are presented in a gray-scale map [Figure 5(a)–(c)]. First, if we look at a dc differential conductance map [Figure 5(a)], it shows that, as the gate voltage increases, a number of lines forming a diamond-like structure emerge from the nonconducting background (black) as V_g increases from –0.64 V. These characteristic features correspond to the formation of a Coulomb blockade dot—conductance is strongly suppressed everywhere except for the regions where the dot population changes. This information revealed by the differential conductance map, however, does not shed any light on charging events that do not contribute to the conductance. That is where the RFR technique comes in handy.

Transport spectroscopy is a characterization technique where electron transport through the sample is measured as a function of one or more parameters.

Figure 5(b) and (c) shows the amplitudes of signals reflected from the drain and gate, respectively. These reflectance maps make visible many additional features

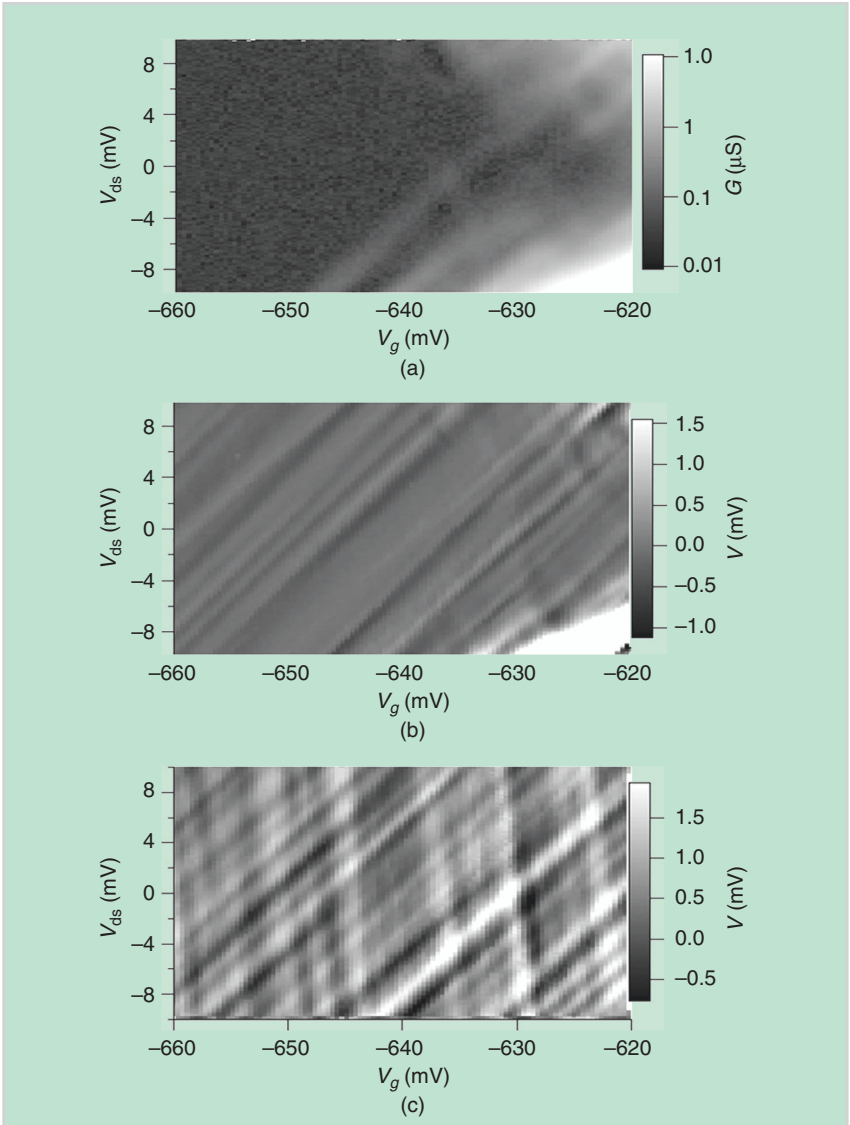

FIGURE 5 An experiment with a short-channel HJFET at T ≈ 3.5 K. (a) A "DC" differential conductance "map." The map of the magnitude of signal reflected from (b) the drain, dG_{drain}/dV_g, and (c) from the gate, dG_{gate}/dV_g.

that stay obscured in the conductance map [Figure 5(a)]. In particular, for the regions in Figure 5(a) where the conductance drops below the noise floor, two sets of lines are still clearly visible: one with positive slopes, $\alpha = dV_{ds}/dV_g > 0$, and another with negative slopes, $\beta < 0$. (Strictly speaking, since the derivatives $d\Gamma/dV_g$ of the peaks in reflectance Γ are measured, for each peak, we observe two features: a peak and a valley. For simplicity, we will refer to each double line feature as a line.) Most notably, while lines of both types are visible in the signal reflected from the gate, only lines with a positive slope are visible in the drain-reflected signals.

To explain these observations, we turn to recent experiments where charging of the Coulomb-blockaded states that do not contribute to conductance was detected by RFR [15], [16]. The observed lines are identified as charge population changes in the Coulomb-blockaded objects: in this process, a small amount of power is dissipated along with the capacitance change [17], leading to small but detectable changes in the magnitude and phase of the reflected signals. The slopes of these lines are defined by the capacitive coupling from the charging states to a respective electrode [26] so that $\alpha = dV_{ds}/dV_g = C_g/(C_g + C_s)$ and $\beta = -C_g/C_d$. Here, C_g, C_s, and C_d are capacitances from the Coulomb-blockaded object to the gate, source, and drain electrodes, respectively. When the Fermi level in the drain electrode is aligned with the electrochemical potential in the charging object, single-electron charging occurs near the drain. This corresponds to the lines with positive slopes (α); charging occurring near the source corresponds to the lines with negative slopes (β). When an RF signal comes from the gate, the detected change in the reflection comes from electron population change near both the source and the drain, and, thus, we observe both types of lines.

Conversely, for an RF signal applied from the drain side, only lines with positive slope, associated with charging near the drain only, are observed in the reflected signal. This is expected since near the threshold, where the conductance between the source and drain is very low, the charging of the states capacitively coupled to the (grounded) source is less likely to respond to the RF signals applied to the drain. Only when the conductance through the channel increases ($V_g > -0.635$ V), a few faded lines with a negative slope also emerge in the drain-reflected signal. The values of $\alpha \approx 0.8$ and $\beta \approx -6$ indicate that charging objects in this case have a stronger coupling to the gate than to the source or drain. Taking into account the geometry of the sample (i.e., a large area where isolated puddles of charge might form), we attribute the majority of the observed lines in a range of V_g where the channel is nearly completely depleted to single-electron charging of isolated puddles.

The results of the experiment presented in Figure 5 demonstrate that the proposed RFR technique reveals complementary information necessary for the identification of spatially separated charging processes guided by a Coulomb blockade.

DUAL-PORT RFR FOR NANOSCALE Si METAL-OXIDE-SEMICONDUCTOR SET

After confirming the validity of the proposed technique on a convenient model system, we applied it for an investigation of charging of the few first charged states in ultrasmall Si SHTs. The devices are fabricated using nanowires on Si-on-insulator (SOI) complementary metal-oxide semiconductor technology [27].

This advanced process on 300-mm SOI wafers has been developed to meet the requirements for the end of the International Technology Roadmap for Semiconductors [28] near the 7-nm node. Here, the channel forming the SHT island is 25 nm long, 15 nm wide, and 11 nm thick. The nanowire is etched away from the SOI film (mesa isolation) and covered by a bilayer gate oxide made of a few angstroms of silicon dioxide and then several nanometers of hafnium silicon oxynitride (HfSiON). The gate overlaps the wire (see Figure 6) and is made of a first layer of titanium nitride (TiN), followed by polycrystalline Si. This complex set of materials was introduced in microelectronics to meet the scaling requirements, but it is also a well-known source of charge traps, especially at the interfaces between different materials.

In contrast to the experiment with an HJFET described previously, in which the formation of the Coulomb-blockaded puddles is a matter of chance and results from random potential fluctuations, the formation of the island in the SHT is the result of careful device design. Yet, there are possibilities for fabrication defects leading to deviations from the ideal device behavior. Figure 7 shows the measured results for the SHT described previously. The first map in Figure 7(a) shows a differential conductance versus V_g and V_{ds}. In the range $-0.85\ \text{V} < V_g < -0.65\ \text{V}$, there are nine easily identifiable Coulomb diamonds, where each diamond corresponds to a stable charge configuration on the SHT quantum dot and single-electron charging occurring (single hole, in this case) at the border crossings. For $V_g > -0.65\ \text{V}$, the conductance signal drops below the noise floor. As a guide for the eye, we draw a line indicating the first hole that is observable in the conductance map. But is there a way to determine when the very first hole enters the dot?

Let us now turn to the reflectometry maps. These maps are measured at the two device ports, the gate and the drain, respectively, and each consists of two components of the reflected signals (R and Θ). Figure 7(b) and (c) represents the signals reflected from the drain; Figure 7(d) and (e) represents the signals reflected from the gate of the SHT. In the area of the map situated to the left from the tilted dashed line, there is a clear match between the diamond pattern in the conductance, Figure 7(a), and charge transitions delineated by the experimentally obtained lines in the reflected signals [Figure 7(b)–(e)]. In this region, two distinctly different sets of lines can be identified in the reflection maps: 1) tilted lines with a slope $\alpha = dV_g/dV_{ds} \sim 1$, visible in Figure 7(b) and (d), and 2) nearly vertical lines with a slope $\beta = dV_g/dV_{ds} \sim -\infty$, which are observable in the gate reflection shown in Figure 7(c) down to $V_g \sim -0.78\ \text{V}$, but

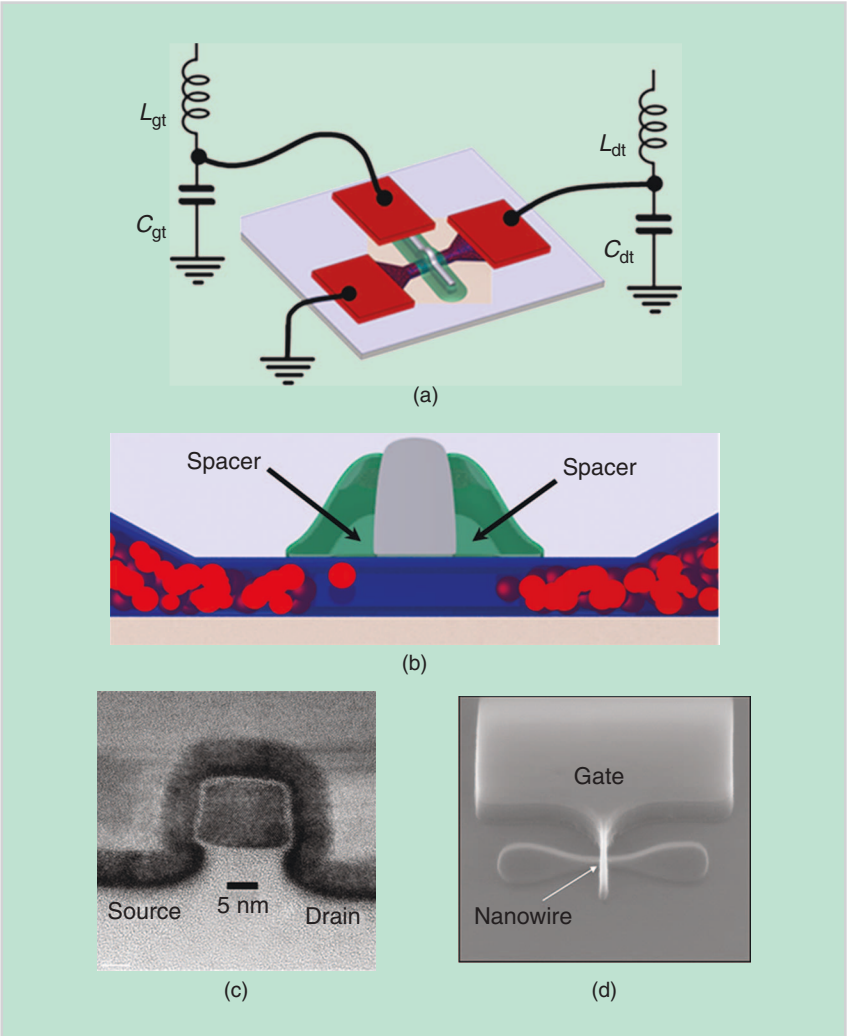

FIGURE 6 The Si SHT experiment: (a) a simplified diagram of the device test circuit, (b) a cross section with implanted donor atoms (the spacers above undoped regions are acting as tunnel barriers), (c) an SEM micrograph of a cross section of an Si SET, and (d) a side view of the device with a gate overlapping the nanowire.

RFR-based spectroscopy offers a versatile spectroscopic tool that is particularly useful for the identification of single-electron charging in nanoscale devices.

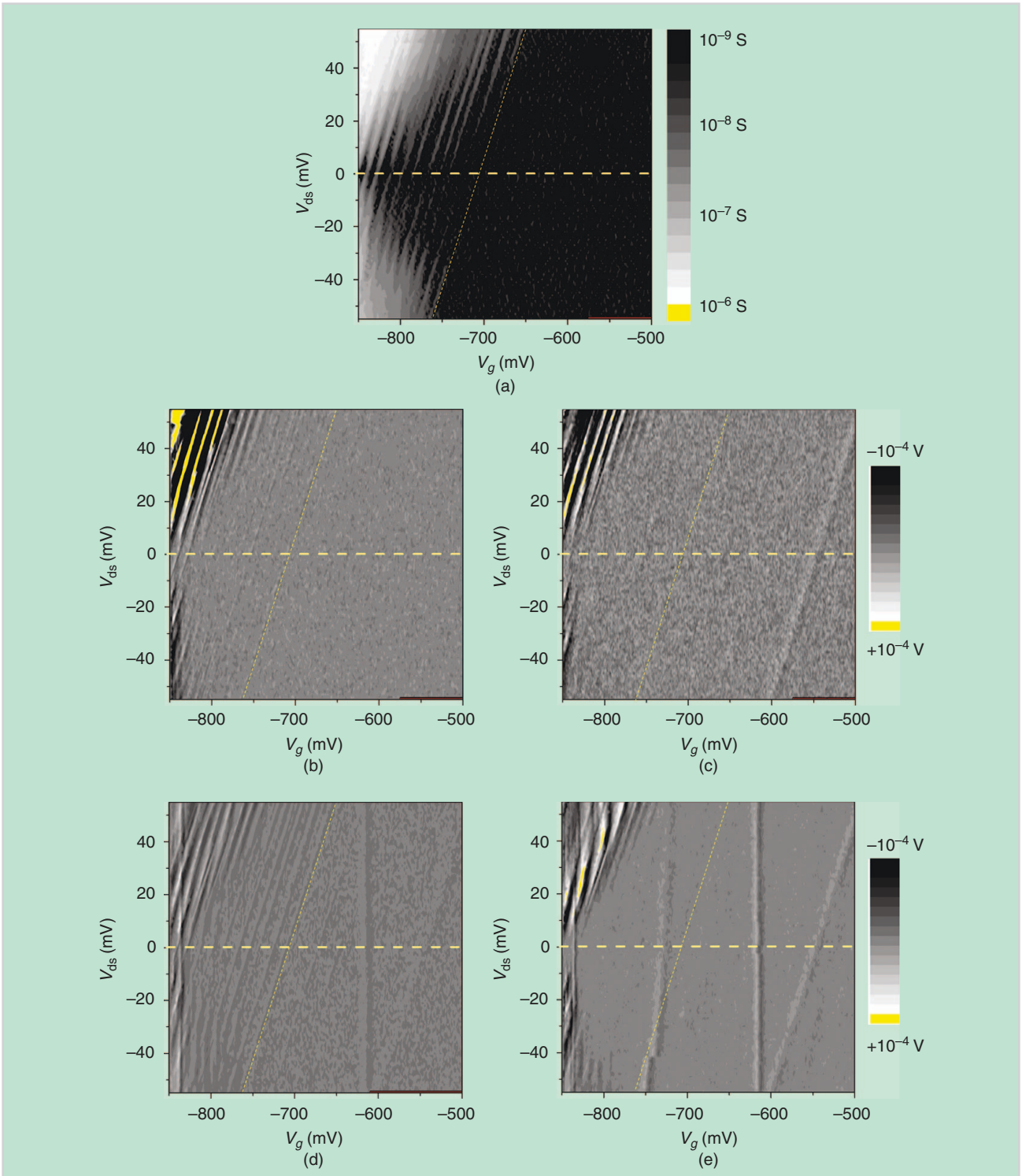

FIGURE 7 The experimental results obtained for Si SHT. (a) The differential conductance (plotted in log scale) with black corresponding to low conductance. Maps of the magnitude and phase of the signals reflected from (b), (c) the drain $d\Gamma_{drain}/dV_g$ and (d), (e) the gate, $d\Gamma_{gate}/dV_g$. The carrier frequencies are $f_d = 453$ MHz, and $f_g = 319$ MHz. The dashed tilted line is a guide for the eye to delineate the first charge transition detectable by the low-frequency transport spectroscopy technique.

are not clearly visible in drain reflections [Figure 7(b)]. By applying the same analysis as used for Figure 5, we identify the single-hole charging processes occurring in the SHT device as follows. First, from the values of α and β, we conclude that in this device $C_s, C_d \ll C_g$, as expected from the device design.

As mentioned previously, the nearly vertical, negatively sloped β-lines are attributed to the charge exchange occurring near the grounded source, and positively sloped

α-lines correspond to single-electron charge transitions occurring near the drain of the device. There are four α-lines with a slope ≈ 1 in Figure 7(b) and (d) at $V_g > -0.76$ V that have no matching vertical lines, yet they are still associated with charge transfers through the dot, which is indicated by a measurable conductance for these lines on the low-frequency conductance map [Figure 7(a)] at a high source–drain bias.

On closer inspection, however, it can be seen that two more lines with the same slope ≈ 1 can be identified in the plot of gate reflection magnitude [Figure 7(d)]. These lines cross the $V_{ds} = 0$ axis at $V_g \approx -0.67$ V and ≈ -0.64 V in a region where the dc conductance is below the measurement noise floor. These are likely the very first holes that are contributing to the population of the island. The poor contrast (i.e., the weak signal) observed for these transitions can be attributed to very low tunneling rates associated with these charging events due to the very large source and drain barrier resistances. Nonetheless, the reflectometry technique enables resolving and identifying these transitions.

The previous observations indicate that the population of the dot in this particular device begins with an easier charge exchange between the dot and the drain, so charge transfer through the dot is limited primarily by the source junction, which has a larger resistance under these conditions. The correspondingly lower tunnel rate at the source leads to an immeasurably small change in the reflection associated with the charge transfer at the source, and, consequently, no vertical lines are observed even in the gate-reflected signal. After the first few holes are added to the dot, the charging (and associated dissipation) on the source side becomes detectable in the gate-reflected signal, leading to the appearance of β-sloped lines, along with α-sloped lines and ultimately closed Coulomb diamonds.

But the reflectometry signals also reveal that—in addition to SHT dot charging—other charging events can be detected and identified well below the onset of conductance through the dot. These additional charging events appear to be unrelated to SHT dot charging. We now consider three such features in Figure 7(b)–(e).

First, there is a vertical line with a large magnitude appearing near $V_g = -0.605$ V clearly visible in the gate reflection signal. The fact that this line is vertical indicates a complete decoupling from the drain of the device. Second, there is a line with a positive slope $\alpha \sim 3$, which is only visible in the phase map of the gate-reflected signal [Figure 7(e)] near $V_g = -0.72$ V.

As we had previously shown [15], the lines with a slope $\alpha > 1$ correspond to the charging of objects extrinsic to the main dot of the device. For example, it could be a dopant located near the source and very weakly capacitively coupled to the drain. Alternatively, it can be a charged defect, tunnel-coupled to the gate [15] and asymmetrically capacitevely coupled to the source and drain electrodes, so that the drain voltage has only very minor influence on this charging process. Neither of these two lines is visible in the drain-coupled signal, indicating that these particular charging objects are far away from the drain. The third line, which is visible in Figure 7(c)–(e), has a slope of $\alpha \sim 1$ and it crosses the $V_{ds} = 0$ at $V_g = -0.55$ V. The fact that it becomes visible not only in the gate-reflected signal but also in the drain-reflected signal indicates that it originates from charging events occurring in closer proximity to the drain. This characteristic suggests that it could be a dopant located near the drain and capacitively coupled to the gate. The predominance of phase change for the second and third charging objects is indicative of a predominantly capacitive load on the tank circuit [19] [Figure 1(b)] and may correspond to a change in the differential capacitance during charge switching, although a more detailed analysis is required to unambiguously resolve this.

CONCLUSION

To summarize, we proposed and implemented a charge detection technique that enables spatial identification of the charging processes in mesoscopic systems. In contrast to the previously reported experiments, this technique enables one to distinguish between charging mechanisms corresponding to charge transport through the channel and charging processes that do not contribute to charge transfer between the source and the drain. In addition, the analysis of the combined reflected signals holds promise for improving understanding of the details of charging mechanisms, including the issues of Sisyphus resistance [14] and quantum capacitance [29].

Electron transport in a heterojunction FET with a short and wide gate offers an opportunity to study a number of interesting physical processes near the conductance threshold.

ACKNOWLEDGMENTS

This work was supported by National Science Foundation grant DMR-1207394. X. Jehl and M. Sanquer acknowledge financial support from the European Union through the FP7 Future and Emerging Technologies initiatives under the Towards Low Power (TOLOP) and Silicon at Atomic and Molecular Scale (SiAM) projects. We are grateful to Michael McConnell for reading the manuscript and making useful suggestions.

ABOUT THE AUTHORS

Alexei O. Orlov (aorlov@gmail.com) received his Ph.D. degree in physics from the Institute of Radio Engineering and Electronics of the Russian Academy of Sciences, Moscow, in 1990. He is currently a research professor in the Department of Electrical Engineering at the University of Notre Dame. His research interests

include experimental studies of quantum-dot cellular automata and single-electron devices, nanoscaled infrared antenna-coupled sensors, and nanomagnetics logic. He has authored or coauthored more than 100 articles in refereed scientific journals. He is a Member of the IEEE.

Patrick Fay (pfay@nd.edu) received his Ph.D. degree in electrical engineering from the University of Illinois at Urbana-Champaign in 1996. He is currently a professor in the Department of Electrical Engineering at the University of Notre Dame. His research interests include the design, fabrication, and characterization of electronic and optoelectronic devices and circuits from RF through the millimeter-wave regime. He has published eight book chapters and more than 100 articles in refereed scientific journals. He is a Senior Member of the IEEE.

Gregory L. Snider (gsnider@nd.edu) received his Ph.D. degree in electrical engineering from the University of California, Santa Barbara, in 1991. He is currently a professor in the Department of Electrical Engineering at the University of Notre Dame. His research interests are in the areas of device physics, nanoelectronics, and nanofabrication. He has authored or coauthored more than 100 journal papers and currently serves as an associate editor for *IEEE Transactions on Electronic Devices*. He is a Senior Member of the IEEE.

Xavier Jehl (xavier.jehl@cea.fr) received his Ph.D. degree in physics from the Université Fourier, Grenoble, France, in 1999. While working on his doctoral degree, he was with the Atomic Energy Council (CEA), Grenoble, where he was involved in the experimental detection of doubled shot noise in mesoscopic superconductor/normal metal contacts. Since 2002, he has been working in the fundamental science division of CEA-Grenoble in close collaboration with the advanced complementary metal–oxide–semiconductor (CMOS) facility of CEA-LETI. His current topics of interest are silicon-based electron pumps, single-dopant nanoelectronics, and radio-frequency reflectometry.

Sylvain Barraud (sylvain.barraud@cea.fr) received his Ph.D. degree from the Paris-Sud University, Orsay, France, in 2001. In November 2001, he joined CEA-LETI-MINATEC, Grenoble, France, as a research staff member. Since 2010, he has been involved in advanced CMOS process integration.

Marc Sanquer (marc.sanquer@cea.fr) received his Ph.D. degree in physics from the Paris-Sud-Orsay University in 1985. He is currently the head of the laboratory for quantum electronic transport and superconductivity in the Institute for Nanosciences and Cryogeny at the Atomic Energy Council-Grenoble/University of Grenoble-Alpes, France. He has authored or coauthored more than 150 articles in refereed scientific journals.

REFERENCES

[1] P. Smith, C. Furse, and J. Gunther, "Analysis of spread spectrum time domain reflectometry for wire fault location," *IEEE Sensors J.*, vol. 5, no. 6, pp. 1469–1478, Dec. 2005.

[2] R. Notarpietro, S. De Mattia, M. Campanella, Y. Pei, and P. Savi, "Detection of buried objects using reflected GNSS signals," *EURASIP J. Adv. Signal Process.*, no. 1, pp. 132–145, 2014.

[3] B. P. Mohanty, "Soil hydraulic property estimation using remote sensing: A review," *Vadose Zone J.*, vol. 12, no. 4, 2013.

[4] J. Zhuang and J. F. Kolb, "Time domain dielectric spectroscopy of nanosecond pulsed electric field induced changes in dielectric properties of pig whole blood," *Bioelectrochemistry*, no. 103, pp. 28–33, June 2015.

[5] R. J. Schoelkopf, P. Wahlgren, A. A. Kozhevnikov, P. Delsing, and D. E. Prober, "The radio-frequency single-electron transistor (RF-SET): A fast and ultrasensitive electrometer," *Science*, vol. 280, no. 5367, pp. 1238–1242, May 1998.

[6] M. C. Cassidy, A. S. Dzurak, R. G. Clark, K. D. Petersson, I. Farrer, D. A. Ritchie, and C. G. Smith, "Single shot charge detection using a radio-frequency quantum point contact," *Appl. Phys. Lett.*, vol. 91, no. 22, pp. 222104–222107, 2007.

[7] A. M. Tyryshkin, S. Tojo, J. J. L. Morton, H. Riemann, N. V. Abrosimov, P. Becker, H.-J. Pohl, T. Schenkel, M. L. W. Thewalt, K. M. Itoh, and S. A. Lyon, "Electron spin coherence exceeding seconds in high-purity silicon," *Nat. Mater.*, vol. 11, no. 2, pp. 143–147, 2012.

[8] K. Saeedi, S. Simmons, J. Z. Salvail, P. Dluhy, H. Riemann, N. V. Abrosimov, P. Becker, H.-J. Pohl, J. J. L. Morton, and M. L. W. Thewalt, "Room-temperature quantum bit storage exceeding 39 minutes using ionized donors in Silicon-28," *Science*, vol. 342, no. 6160, pp. 830–833, 2013.

[9] J. T. Muhonen, J. P. Dehollain, A. Laucht, F. E. Hudson, R. Kalra, T. Sekiguchi, K. M. Itoh, D. N. Jamieson, J. C. McCallum, A. S. Dzurak, and A. Morello, "Storing quantum information for 30 seconds in a nanoelectronic device," *Nat. Nano*, vol. 9, pp. 986–991, 2014.

[10] L. Roschier, P. Hakonen, K. Bladh, P. Delsing, K. W. Lehnert, L. Spietz, and R. J. Schoelkopf, "Noise performance of the radio-frequency single-electron transistor," *J. Appl. Phys.*, vol. 95, no. 3, pp. 1274–1286, 2004.

[11] L. P. Kouwenhoven, D. G. Austing, and S. Tarucha, "Few-electron quantum dots," *Rep. Progr. Phys.*, vol. 64, no. 6, p. 701, 2001.

[12] M. Hofheinz, X. Jehl, M. Sanquer, G. Molas, M. Vinet, and S. Deleonibus, "Detection of individual traps in silicon nanowire transistors," in *Book Detection of Individual Traps in Silicon Nanowire Transistors*. Institute of Electrical and Electronics Engineers Computer Society, 2005, pp. 225–228.

[13] H. D. Cheong, T. Fujisawa, T. Hayashi, Y. Hirayama, and Y. H. Jeong, "Impedance analysis of a radio-frequency single-electron transistor," *Appl. Phys. Lett.*, vol. 81, no. 17, pp. 3257–3259, 2002.

[14] F. Persson, C. M. Wilson, M. Sandberg, G. Johansson, and P. Delsing, "Excess dissipation in a single-electron box: The Sisyphus resistance," *Nano Lett.*, vol. 10, pp. 953–957, 2010.

[15] B. J. Villis, A. O. Orlov, X. Jehl, G. L. Snider, P. Fay, and M. Sanquer, "Defect detection in nano-scale transistors based on radio-frequency reflectometry," *Appl. Phys. Lett.*, vol. 99, no. 15, pp. 152106–152103, 2011.

[16] B. J. Villis, A. O. Orlov, S. Barraud, M. Vinet, M. Sanquer, P. Fay, G. Snider, and X. Jehl, "Direct detection of a transport-blocking trap in a nanoscaled silicon single-electron transistor by radio-frequency reflectometry," *Appl. Phys. Lett.*, vol. 104, no. 23, pp. 233503–233505, 2014.

[17] C. Ciccarelli and A. J. Ferguson, "Impedance of the single-electron transistor at radio-frequencies," *New J. Phys.*, vol. 13, no. 9, p. 093015, 2011.

[18] J. Verduijn, M. Vinet, and S. Rogge, "Radio-frequency dispersive detection of donor atoms in a field-effect transistor," *Appl. Phys. Lett.*, vol. 104, no. 10, pp. 102104–102107, 2014.

[19] M. F. Gonzalez-Zalba, S. Barraud, A. J. Ferguson, and A. C. Betz, "Probing the limits of gate-based charge sensing," *Nat. Commun.*, vol. 6, Article No. 6084, 2015.

[20] J. A. Nixon, J. H. Davies, and H. U. Baranger, "Breakdown of quantized conductance in point contacts calculated using realistic potentials," *Phys. Rev. B*, vol. 43, no. 15, pp. 12638–12641, 1991.

[21] M. E. Raikh and I. M. Ruzin, "Fluctuations of the hopping conductance of one-dimensional systems," *J. Exp. Theoret. Phys.*, vol. 68, no. 3, pp. 642–647, 1989.

[22] A. Orlov, M. Raikh, I. Ruzin, and A. K. Savchenko, "Distribution function of hopping conductance fluctuations of a short GaAs field effect transistor channel," *Solid State Commun.*, vol. 72, no. 2, pp. 169–172, 1989.

[23] J. Weis, R. J. Haug, K. V. Klitzing, and K. Ploog, "Transport spectroscopy of a confined electron system under a gate tip," *Phys. Rev. B*, vol. 46, no. 19, pp. 12837–12840, 1992.

[24] V. V. Kuznetsov, A. K. Savchenko, D. R. Mace, E. H. Linfield, and D. A. Ritchie, "Resonant tunneling spectroscopy of interacting localized states: Observation of the correlated current through two impurities," *Phys. Rev. B*, vol. 56, no. 24, pp. 15533–15536, 1997.

[25] A. O. Orlov, A. K. Savchenko, A. S. Rylik, B. A. Malak'hov, and N. A. Sinev, "Ballistic transport through the fluctuation potential: Strong one-dimensional quantization in two-dimensional GaAs/AlGaAs structures," *J. Phys. B*, vol. 6, no. 26, p. 349, 1994.

[26] K. K. Likharev, "Single-electron devices and their applications," *Proc. IEEE*, vol. 87, pp. 606–632, 1999.

[27] S. Barraud, R. Lavieville, C. Tabone, F. Allain, M. Cassex, M. P. Samson, V. Maffini-Alvarro, and M. Vinet, "Strained silicon directly on insulator N- and P-FET nanowire transistors," in *Book Strained Silicon Directly on Insulator N- and P-FET Nanowire Transistors*, pp. 65–68, 2014.

[28] ITRS, International Technology Roadmap for Semiconductors. (2009). [Online]. Available: http://www.itrs.net/links/2009ITRS/Home2009.htm

[29] K. D. Petersson, C. G. Smith, D. Anderson, P. Atkinson, G. A. C. Jones, and D. A. Ritchie, "Charge and spin state readout of a double quantum dot coupled to a resonator," *Nano Lett.*, vol. 10, no. 8, pp. 2789–2793, 2010.

N